Available online at sjuoz.uoz.edu.krd

Science Journal of University of Zakho

Vol. 13, No.4 pp520–531October-December,2025

p-ISSN: 2663-628X
e-ISSN: 2663-6298

GREEN-SYNTHESIZED ZINC OXIDE NANOPARTICLES FROM VERJUICE (*Vitis vinifera*) EXHIBIT HEPATOPROTECTIVE AND ANTIOXIDANT EFFECTS AGAINST CARBON TETRACHLORIDE -INDUCED TOXICITY IN MALE RATS

Pola Z. Aziz [1, *], and Treefa F. Ismail [1]

[1] Department of Biology, College of Education, Salahaddin University-Erbil, Kurdistan Region, Iraq

*Corresponding author email: pola.aziz@su.edu.krd

Received: 21 Jun 2025 Accepted:25 Jul 2025 Published: 04 Oct 2025 https://doi.org/10.25271/sjuoz.2025.13.4.1633

ABSTRACT:

Drug-induced liver injury, particularly that caused by carbon tetrachloride (CCl_4), poses significant clinical challenges due to oxidative stress and limited therapeutic options. This study investigated the hepatoprotective and antioxidant potential of green-synthesized zinc oxide nanoparticles (ZnO-NPs) using verjuice extract from unripe grapes in a CCl_4–induced rat model. The ZnO-NPs were characterized using UV-visible spectroscopy, X-ray diffraction, fourier transform infrared (FTIR) scanning electron microscopy, and energy-dispersive X-ray spectroscopy (EDX) analyses. Twenty male Wistar rats were assigned to four groups: control, CCl_4 toxicity (1 mL/kg twice weekly for 4 weeks), co-treatment (CCl_4 + ZnO-NPs 50 mg/kg daily for 4 weeks), and ZnO-NP post-treatment (CCl_4 for 4 weeks followed by ZnO-NPs 50 mg/kg daily for 4 weeks). ZnO-NPs significantly restored superoxide dismutase (SOD) activity and decreased malondialdehyde (MDA) levels to near control values, while normalizing alanine aminotransferase (ALT), aspartate aminotransferase (AST), and alkaline phosphatase (ALP) activities. Histopathological evaluation confirmed near-complete recovery of hepatic and renal architectures. These results demonstrate that verjuice-synthesized ZnO-NPs exert potent antioxidant and regenerative effects through the preservation of endogenous defenses and promotion of tissue repair, and the green synthesis approach offers an eco-friendly, biocompatible nanotherapeutic strategy with promising applications for drug-induced liver injury.

KEYWORDS: Carbon tetrachloride, Green synthesis, Hepatoprotection, Liver function, Oxidative stress biomarkers, Superoxide dismutase.

1. INTRODUCTION

The liver serves as the primary metabolic hub for both endogenous compounds and xenobiotic substances, making hepatic function critical for maintaining physiological homeostasis. Disruption of liver metabolism is intrinsically linked to hepatocellular damage, contributing to the pathogenesis of various liver disorders, including cirrhosis, hepatitis, and alcoholic liver disease(Conde de la Rosa *et, al.*, 2022; Mohajan, 2025). Environmental toxicants and chemical pollutants, particularly carbon tetrachloride (CCl_4), thioacetamide, ethanol, and acetaminophen, represent major etiological factors in hepatotoxicity. The predominant mechanism underlying chemical-induced liver injury involves the buildup of reactive oxygen species (ROS), which subsequently triggers oxidative stress and cellular damage (Hashim *et, al.*, 2025).

Carbon tetrachloride has emerged as a prototypical hepatotoxin extensively utilized in experimental models to induce liver injury and evaluate potential hepatoprotective interventions (Mohi-Ud-Din *et, al.*, 2019). CCl_4 undergoes biotransformation via cytochrome P450 enzymes to generate reactive metabolites that initiate hepatocellular damage through oxidative stress and inflammatory cascades (Szymonik-Lesiuk *et, al.*, 2003; Weber *et, al.*, 2003). Despite substantial advances in hepatology, effective management of liver diseases remains challenging for modern medicine, requiring the exploration of alternative therapeutic approaches (Wazir *et, al.*, 2023)

Natural products have garnered considerable attention as potential hepatoprotective agents due to their multifaceted mechanisms of action and favorable safety profiles (Datta *et, al.*, 2023; Fazal *et, al.*, 2024). Grapes (*Vitis vinifera*) represent a rich source of bioactive compounds, including phenolic acids, flavonoids, and anthocyanins, which collectively contribute to their antioxidant properties (Zhou *et, al.*, 2022). In traditional Iranian medicine, unripe grape juice, known as "verjuice" or "ghureh," has been historically employed for managing hypertension and obesity (Nematbakhsh *et, al.*, 2013). This acidic extract, derived from immature grapes, contains elevated concentrations of polyphenolic compounds that exhibit potent antioxidant activity (Salah Eddine *et, al.*, 2020). The cardiovascular protective effects of grape-derived compounds have been attributed to their polyphenolic constituents, which demonstrate significant ROS scavenging capacity and prevent biomolecular oxidation (Dohadwala & Vita, 2009; Dhalaria *et, al.*, 2020). Recent investigations have validated the lipid-lowering and antihypertensive properties of unripe grape juice,

* Corresponding author

supporting its traditional therapeutic applications (Alipour *et, al.*, 2012; Bayram & Elgin Karabacak, 2022).

The convergence of nanotechnology and medicine has given rise to "nanomedicine," offering innovative approaches for disease diagnosis, treatment, and monitoring (Park *et, al.*, 2025). Zinc oxide nanoparticles (ZnO-NPs) have emerged as versatile nanomaterials with significant antioxidant activity and hepatoprotective potential through their ability to mitigate oxidative stress (Gulab *et, al.*, 2024). Contemporary research emphasizes green synthesis methodologies for nanoparticle production to minimize toxicity concerns and enhance biocompatibility (Kirubakaran *et, al.*, 2025).

The green synthesis of ZnO-NPs using unripe grapes represents a novel, environmentally sustainable approach where abundant bioactive compounds (polyphenols, flavonoids, and organic acids) serve dual functions as reducing and capping agents (Saratale *et, al.*, 2020). These phytochemicals not only facilitate the formation of stable ZnO-NPs but may also enhance their biological activity, potentially amplifying their antioxidant and hepatoprotective efficacy (Ashraf *et, al.*, 2023).

Green synthesis using plant extracts offers enhanced biocompatibility and reduced toxicity compared to chemical methods by eliminating toxic reducing agents and harsh conditions. The phytochemicals in unripe grapes (gallic acid, catechins, and proanthocyanidins) serve dual functions as reducing agents for zinc ion transformation and natural capping agents for particle stability, while potentially providing additional therapeutic benefits (Fiedot-Toboła *et, al.*, 2021; Udayagiri *et, al.*, 2024).

Furthermore, the size, morphology, and surface characteristics of green-synthesized ZnO-NPs can be modulated by optimizing extraction parameters and synthesis conditions, enabling their customization for therapeutic applications (El-Saadony *et, al.*, 2024). The bioactive coating derived from grape phytochemicals may enhance cellular uptake and bioavailability while reducing potential toxicity associated with bare nanoparticles (Al-Sulivany *et, al.*, 2024; Zhao *et, al.*, 2020).

.

Recent studies have demonstrated that plant extract-mediated synthesis produces nanoparticles with superior antioxidant activity compared to chemically synthesized counterparts, attributed to the synergistic interaction between the nanoparticle core and bioactive surface coating (Adeyemi *et, al.*, 2022).

Oxidative stress markers such as MDA, SOD, and glutathione (GSH) are widely used to evaluate the balance between free radical generation and antioxidant defense mechanisms in the liver. In addition, liver function tests, including serum ALT, AST, ALP, and bilirubin levels, are essential biochemical indicators for assessing hepatocellular integrity and functional recovery following toxic injury. Therefore, this study aimed to synthesize ZnO nanoparticles using verjuice (*Vitis vinifera*) and to evaluate their hepatoprotective and antioxidant effects against CCl_4-induced liver toxicity in male rats.

2. MATERIALS AND METHODS

Study Design and Workflow:

The experimental workflow comprised three phases: nanoparticle synthesis, animal experimentation, and analytical evaluation (Fig. 1). Fresh unripe grapes were processed to extract verjuice for ZnO-NP synthesis via controlled precipitation, followed by calcination and characterization using UV-Vis, Fourier Transform Infrared (FTIR), Scanning Electron Microscopy (SEM), X-ray Diffraction (XRD), and energy-dispersive X-ray spectroscopy (EDX) analyses. Male Wistar rats underwent CCl_4-induced hepatotoxicity, and subsequently treated with or without ZnO-NP treatment (50 mg/kg, oral gavage). Following the treatment period, animals were sacrificed, and blood and liver tissue were collected for analysis. Final assessment included automated biochemical analysis of liver enzymes, serum oxidative stress biomarkers, and histopathological examination of liver tissues using hematoxylin and eosin staining

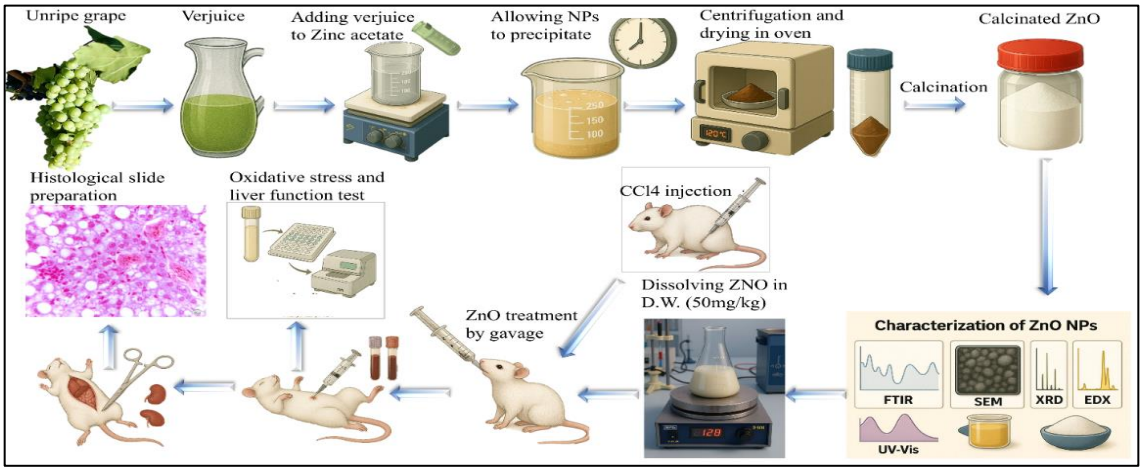

Figure. 1: Schematic representation of the experimental workflow for green synthesis of ZnO-NPs and hepatoprotective evaluation.

Preparation of Verjuice Extract:

Fresh unripe grapes (*Vitis vinifera* L.) were harvested in September 2024 from Erbil Governorate, Iraq. A qualified botanist conducted taxonomic identification and confirmed the plant species. The harvested grapes (2.0 kg) underwent systematic processing under aseptic conditions. Initial washing was performed using running tap water, followed by sterile distilled water rinses. The cleaned grapes were mechanically homogenized using a sterile stainless-steel blender at 15,000 rpm for 3 minutes. The resultant grape mash was subjected to mechanical pressing using a hydraulic press to extract juice

without thermal treatment. Approximately 1.0 L of crude verjuice was obtained and clarified through sequential filtration using sterile cheesecloth and Whatman No. 1 filter paper.

Green Synthesis of ZnO Nanoparticles:

ZnO-NPs were synthesized via controlled precipitation using verjuice as both the reducing and stabilizing agent. The amount of 3.0 g, 13.7 mmol of zinc acetate dihydrate (SDFCL, India) was dissolved in 75 mL of ultrapure water under magnetic stirring at 60°C for 15 minutes. Standardized verjuice (50 mL) was added dropwise at 0.5 mL/min under continuous stirring. The pH was adjusted to 10.0 ± 0.1 using 1 M NaOH solution. Subsequently, the mixture was continuously stirred at ambient temperature for 2 hours. Following this, the mixture was allowed to age undisturbed for 24 hours. The precipitated ZnO-NPs were harvested by centrifugation at 8,000 × g for 15 minutes, washed three times, dried in a vacuum oven at 60°C for 24 hours, and calcined at 500°C for 4 hours.

Physicochemical Characterization:

For UV-visible absorption spectroscopy, an Agilent UV-2600 spectrophotometer (200-800 nm) was used. The Tauc plot approach was utilized to ascertain the ZnO-NPs' optical band gap energy (Eg). The relationship $\alpha = 2.303A/t$, where A is the absorbance and t is the cuvette's path length, was used to get the absorption coefficient (α) from the absorbance data. Plotting $(\alpha h\nu)^2$ against photon energy (hν), where h is Planck's constant and ν is the frequency, created the Tauc graphic. By extending the linear part of the plot to the x-axis intercept, where $(\alpha h\nu)^2 = 0$, which corresponds to the beginning of fundamental absorption, the band gap energy was extrapolated. A Rigaku MiniFlex 600 diffractometer with Cu Kα radiation was used to perform the XRD investigation. The PerkinElmer Spectrum 100 spectrometer (4000-400 cm^{-1}) was used to perform FTIR spectroscopy. The ZnO-NPs' surface shape and elemental makeup were investigated using a Zeiss Sigma 300 field-emission SEM with an integrated EDX detector that was run at 15 kV.

Experimental Animals:

We bought 20 male Wistar albino rats (n = 20) from the Animal Breeding Center at Jihan University in Erbil, Iraq. They were 6–8 weeks old and weighed between 200 and 250 g. The animals were kept in temperature-controlled environments with a 12-hour light/dark cycle, relative humidity of 55 ± 10%, and a temperature of 22 ± 2°C. They also had unlimited access to filtered water and standard laboratory chow. 4.4% sunflower oil, 1.5% limestone, 0.63% salt, 0.158% methionine, 0.062% choline chloride, 25% lysine, 0.05% trace elements, and 66.6% wheat and 25.6% soy make up the typical pellet. (MohamedAmin, 2024).

Experimental Design:

After a 14-day acclimatization period, rats were randomly divided into four groups (n = 5): Group 1 (control) received daily saline (1 mL/kg, p.o.) for 4 weeks; Group 2 (CCl_4 toxicity) received CCl_4 (1 mL/kg, i.p., diluted 1:1 in olive oil) twice weekly for 4 weeks; Group 3 (co-treatment) received CCl_4 injections with concurrent daily ZnO-NPs (50 mg/kg, p.o.) for 4 weeks; and Group 4 (post-treatment) received CCl_4 injections for 4 weeks followed by daily ZnO-NPs (50 mg/kg, p.o.) for an additional 4 weeks. This dose was chosen based on previous rodent studies demonstrating effective biological responses with minimal toxicity (Abbasalipourkabir *et, al.*, 2015).

Sample Collection and Analysis:

At the end of week 4, three groups of rats, and at the end of week 8, the last group were fasted for 12 hours and anesthetized with ketamine-xylazine (9:1 mg/kg, i.p.). Blood samples were obtained via cardiac puncture for biochemical analyses, and liver tissues were excised, weighed, and processed for histopathological slide preparation. Fresh liver tissue samples for histopathological examination were were cut into small pieces, and immediately fixed in 10% neutral buffered formalin for 24-48 hours, then processed through standard histological procedures (dehydration, clearing, paraffin embedding, sectioning, and H&E staining). (Gong *et, al.*, 2008). Oxidative stress biomarkers, malondialdehyde (MDA), superoxide dismutase (SOD), and glutathione (GSH) were measured in serum using colorimetric methods.

Serum levels of GSH, SOD, and MDA were determined using commercial rat-specific enzyme-linked immunosorbent assays (ELISA) kits (BT Lab, Birmingham, UK) following the manufacturer's protocols. Standards and serum samples (100 µL each) were brought to room temperature and added to 96-well microplates pre-coated with specific rat antibodies for each biomarker. Plates were incubated at 37°C for 90 minutes to allow antigen-antibody binding. Wells were washed three times with wash buffer (300 µL per wash) to remove unbound substances. After adding 100 µL of biotinylated detection antibodies and incubating for 60 minutes at 37°C, the mixture was washed. After adding 100 µL of streptavidin-horseradish peroxidase (HRP) conjugate, the mixture was incubated for 30 minutes at 37°C. Following the last washing, 90 µL of 3,3',5,5'-Tetramethylbenzidine (TMB) substrate solution was added, and the mixture was incubated at 37°C for 15 to 30 minutes in the dark until color development took place. 50 µL of stop solution was used to halt the enzymatic reaction, and optical density was immediately measured at 450 nm using an ELISA microplate reader (800TS, BioTek, USA). All samples were analyzed in duplicate, and concentrations were calculated using four-parameter logistic curve fitting.(Marrocco *et, al.*, 2017)

Liver function tests, including alanine aminotransferase (ALT), aspartate aminotransferase (AST), alkaline phosphatase (ALP), and total bilirubin, were analyzed using a cobas c 111 automated biochemical analyzer (Roche Diagnostics, Switzerland). Quality control was performed using appropriate control sera at normal and pathological levels before each run, and the analyzer was calibrated using manufacturer-supplied calibrators according to the standard operating procedures. All measurements were performed in accordance with the manufacturer's instructions and clinical laboratory standards. The hepatosomatic index was calculated as liver weight/body weight × 100 (Gupta *et, al.*, 2017).

$$HSI = \frac{liver\ weight(g)}{body\ weight(g)}(100)$$

Histopathological Examination:

Concurrent with the biochemical assays, histopathological analysis of liver tissue was performed to provide a structural alteration of liver damage and the protective effect of synthesized ZnO-NPs. After the animals were humanely euthanized, liver

specimens were excised and immediately immersed in 10% neutral buffered formalin fixative. The fixed tissues were processed through graded alcohols and xylene and embedded in paraffin. Thin sections (approximately 4–5 µm) were cut and stained with hematoxylin and eosin to visualize hepatic architecture and cellular details. Histology slides were examined under light microscopy and photographed for documentation. The histopathological evaluation focused on comparing liver tissues among the different experimental groups to identify cellular injury, including necrosis, inflammation, and structural degeneration, as well as areas of tissue preservation.

Statistical Analysis:

GraphPad Prism version 9.0 was used to analyze the data, which were presented as mean ± SEM. For intergroup comparisons, the Kruskal-Wallis test with Dunn's test and one-way ANOVA with Tukey's multiple comparison test were employed. The threshold for statistical significance was $p < 0.05$.

3. RESULTS

UV-Visible Absorption Spectroscopy:

Using a Shimadzu UV-2600 double-beam spectrophotometer, UV-visible absorption spectroscopy was used to ascertain the electronic band structure and optical characteristics of the produced nanoparticles. Utilizing aqueous nanoparticle suspensions (0.1 mg/mL) made in ultrapure water, absorption spectra were captured in the 200–800 nm wavelength range and compared to a reference of pure water (Fig. 2). By graphing $(\alpha h\nu)^2$ against photon energy (hv) and projecting the linear part to the x-axis, the optical band gap was determined using the Tauc relation for direct semiconductors.

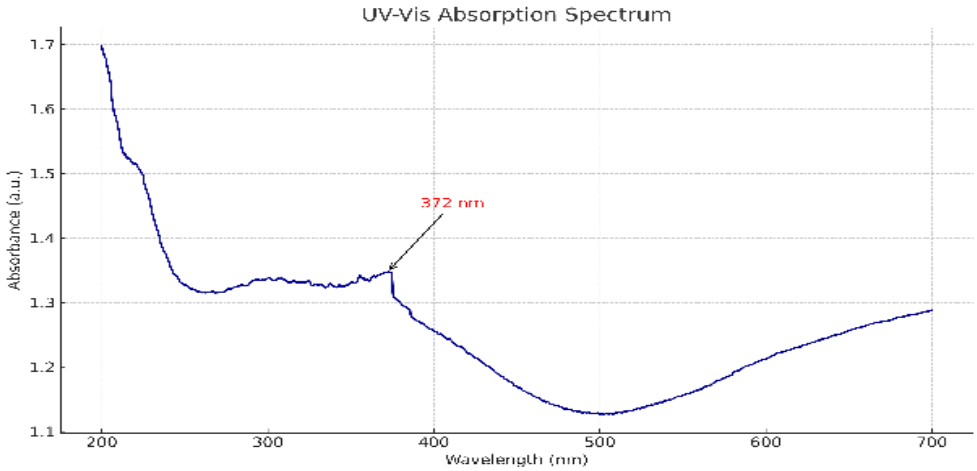

Figure. 2: UV-Vis absorbance spectrum of green-synthesized ZnO-NPs.

X-ray Diffraction Analysis:

According to XRD examination, the pure wurtzite ZnO-NPs phase formed, exhibiting distinctive peaks at 2θ values of 31.7°, 34.4°, 36.2°, 47.5°, 56.6°, 62.8°, and 68.0° (Fig. 3). The crystal planes that the peaks correspond to are (100), (002), (101), (102), (110), (103), and (112), respectively, and they match JCPDS card No. 36-1451. Based on the line broadening of the strongest diffraction peak at 36.2° (101 plane), the average crystallite size was calculated to be 53.1 nm.

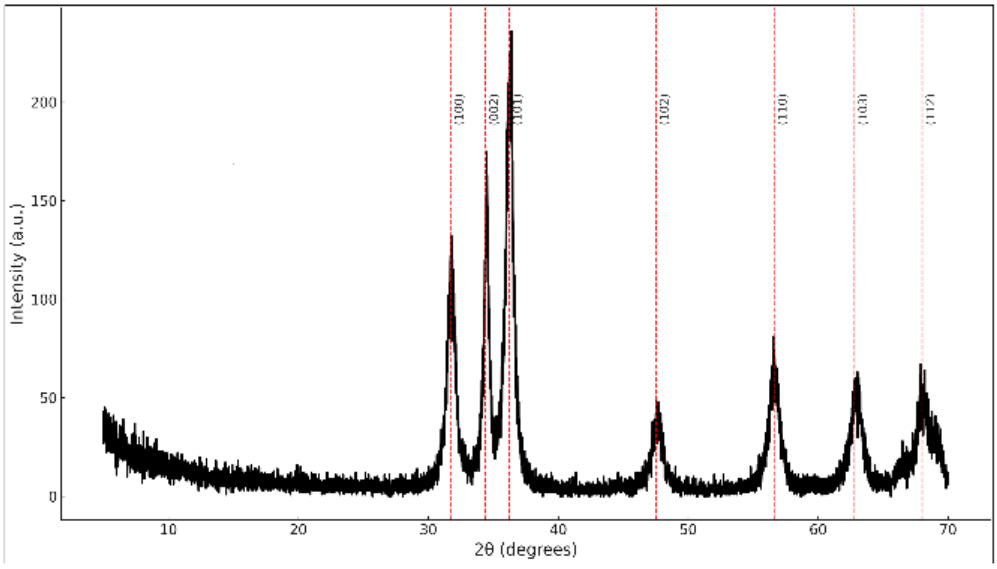

Figure. 3: XRD pattern of green-synthesized ZnO-NPs.

Fourier Transform Infrared Spectroscopy:

Fourier Transform Infrared Spectroscopy (FTIR) analysis showed a broad absorption band at 400-600 cm^{-1}, including a peak at 384 cm^{-1}, which corresponds to Zn–O stretching vibrations, confirming ZnO-NP formation (Fig. 4). Additional peaks at 3400-3500 cm^{-1} (O-H stretching), 1630 cm^{-1} (C=C aromatic stretching), indicated the presence of organic compounds from the verjuice extract acting as capping agents.

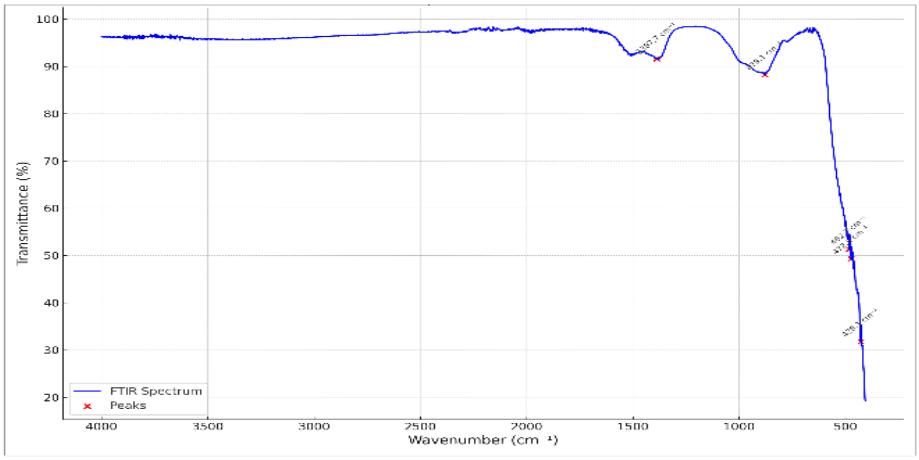

Figure. 4: FTIR spectrum of green-synthesized ZnO-NPs showing Zn–O bond vibrations below 600 cm^{-1} and characteristic bands indicating organic capping agents.

Scanning Electron Microscopy and Energy-Dispersive X-ray Spectroscopy:

Scanning Electron Microscopy SEM) analysis revealed that the nanoparticles exhibited a distinctive flower-like morphology with an average particle size of 85 nm. EDX analysis confirmed the elemental composition, with characteristic peaks for zinc (Zn Lα at 1.01 keV and Zn Kα at 8.63 keV) and oxygen (O Kα at 0.52 keV), indicating high purity with no detectable impurities.

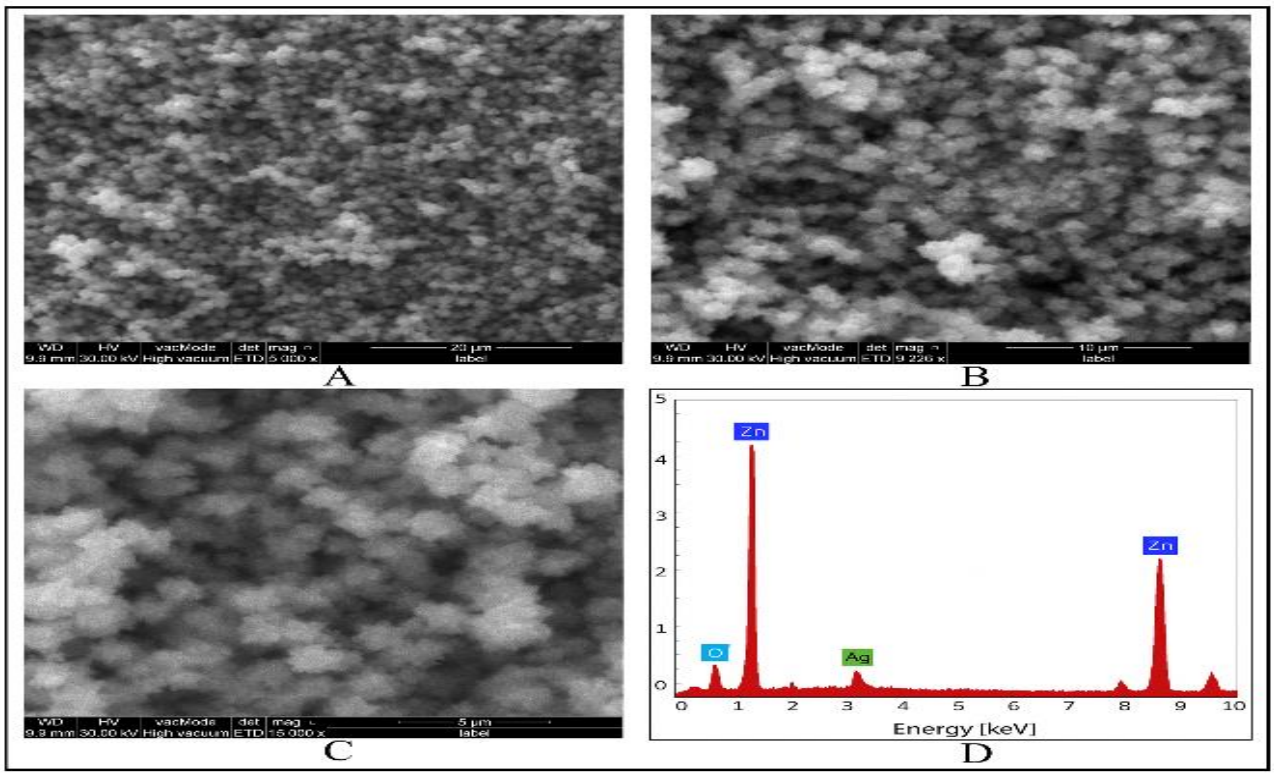

Figure. 5: Morphological and elemental characterization of ZnO-NPs. (A, B) SEM images at 5,000× and 9,000× magnification showing flower-like nanostructures (average size: 85 nm). (C) High-magnification SEM image at 15,000× further detailing the morphology. (D) EDX spectrum confirming the presence of zinc (Zn Lα: 1.01 keV; Zn Kα: 8.63 keV) and oxygen (O Kα: 0.52 keV), with no detectable impurities.

Antioxidant Enzyme Activities:

As presented in Table 1, CCl_4 treatment significantly affected antioxidant enzyme activities relative to controls. The assessment of MDA concentrations as markers of lipid oxidative damage revealed pronounced elevation following CCl_4 exposure compared to untreated controls ($p < 0.0001$). Groups receiving ZnO-NP intervention either concurrently or subsequent to CCl_4 administration exhibited MDA values that approached normal ranges, though with distinct statistical outcomes: co-treatment showed marginal non-significance ($p = 0.0631$). At the same time, post-treatment demonstrated significant normalization ($p = 0.03$) versus controls. These findings suggest ZnO-NP treatment effectively mitigated oxidative stress-induced lipid peroxidation, with complete therapeutic efficacy achieved only in the post-treatment protocol.

The SOD activity was significantly reduced in the CCl_4 group compared to the control group ($p = 0.0014$). The ZnO-NP co-treatment group also demonstrated a significant decrease in SOD activity relative to the control group ($p = 0.0291$). In contrast, ZnO-NP post-treatment resulted in SOD activity levels that were statistically comparable to the control group, with no significant differences observed between these groups ($p = 0.99$).

GSH concentrations showed no statistically significant differences among any of the experimental groups when compared to controls or to each other ($p = 0.37$). All treatment groups, including CCl_4 alone, ZnO-NP co-treatment, and ZnO-NP post-treatment, maintained GSH levels that were statistically similar to the control group.

The statistical analysis revealed distinct patterns of significance across the different antioxidant parameters, with MDA showing the most consistent protective effects from both ZnO-NP treatment protocols. At the same time, SOD recovery was only achieved with post-treatment administration.

Table 1: Effects of ZnO-NP treatment on oxidative stress biomarker levels in the CCl_4-induced hepatotoxicity models.

Parameters	Experimental Groups (Means ± SD)			
	CONTROL	CCl4	ZnO-NP CO.	ZnO-NP POST
MDA (nmol/mg)	1.550 ± 0.454^{b}	2.096 ± 0.194^{a}	1.752 ± 0.15^{ab}	1.559 ± 0.209^{b}
SOD (U/mL)	2.288 ± 0.282^{a}	1.454 ± 0.273^{b}	1.73 ± 0.284^{b}	2.296 ± 0.275^{a}
GSH (µg/mg)	348.7 ± 60.1^{a}	276.5 ± 78.1^{a}	305.3 ± 81.7^{a}	280.9 ± 40.2^{a}

Values are expressed as means ± standard deviation (n = 5 animals per group). The same letter in the rows denotes no significant differences among parameters at $P<0.05$, a combination of letters (e.g., ab) indicates no significant differences from groups labeled either a or b. CCl4: carbon tetrachloride group; ZnO-NP CO.: zinc oxide co-treatment group; ZnO-NP POST: zinc oxide post-treatment group. MDA: malondialdehyde; SOD: superoxide dismutase; GSH: glutathione peroxidase;

Weight Gain Analysis:

The weight gain analysis revealed severe hepatotoxicity-induced growth retardation in the CCl4 group (41.6 ± 12.7 g) compared to controls (97.2 ± 8.5 g), representing a 57.2% reduction in weight gain over the 4-week treatment period. ZnO-NP treatment provided significant hepatoprotective effects, with treated animals achieving 73.6 ± 15.6 g weight gain, which was 77% better than CCl4 alone but still 24.3% below control levels ($P = 0.0299$). The most remarkable finding was observed in the extended 8-week ZnO-NP post-treatment group (100.8 ± 14.7 g).

Hepatosomatic Index (HSI) Analysis:

Control animals maintained normal HSI values of 2.78 ± 0.07%, while CCl_4 treatment induced marked hepatomegaly (4.41 ± 0.20%, 58.6% increase). ZnO-NP co-treatment significantly attenuated hepatomegaly (3.36 ± 0.19%, 20.9% above control), while ZnO-NP post-treatment showed remarkable recovery (2.87 ± 0.17%, 3.2% above control).

Liver Weight Analysis:

Absolute liver weight measurements demonstrated hepatomegaly and tissue damage across experimental groups (Table 2). Control animals exhibited normal liver weights of 9.5 ± 0.3 g with a low coefficient of variation (CV = 3.2%). CCl_4 treatment induced significant hepatomegaly with liver weights of 12.7 ± 1.0 g, representing a 33.7% increase and higher variability (CV = 7.9%), indicating pathological enlargement. ZnO-NP treatment substantially reduced CCl_4-induced hepatomegaly to 10.7 ± 0.7 g (12.6% above control), demonstrating a 63% reduction in liver enlargement compared to CCl_4 alone with intermediate variability (CV = 6.5%). The 2.0 g difference between CCl_4 and ZnO-NP groups represents a clinically significant reduction in hepatomegaly, confirming hepatoprotective effects against CCl_4-induced liver enlargement.

Table 2: Effects of ZnO-NP treatment on body weight gain, hepatosomatic index (HIS), and liver weight parameters in the CCl_4-induced hepatotoxicity models.

Parameters	Experimental Groups (Means ± SD)			
	CONTROL	CCl4	ZnO-NP CO.	ZnO-NP POST
WG (g)	97.2 ± 8.5^{ab}	41.6 ± 12.7^{c}	73.6 ± 15.6^{b}	100.8 ± 14.7^{a}
HIS%	2.78 ± 0.07^{c}	4.41 ± 0.20^{a}	3.36 ± 0.19^{b}	2.87 ± 0.17^{c}
LW (g)	9.5 ± 0.3^{ab}	12.7 ± 1.0^{a}	10.7 ± 0.7^{b}	9.16 ± 0.55^{c}

Values are expressed as means ± standard deviation (n = 5 animals per group). The same letter in the rows denotes no significant differences among parameters at P<0.05, a combination of letters (e.g., ab) indicates no significant differences from groups labeled either a or b. WG for weight gain, HIS for hepatosomatic index, and LW for liver weight.

Liver Function Tests:

The comprehensive biochemical analysis of liver function parameters across all experimental groups was presented in Table 3, revealing distinct patterns of hepatic injury and protection based on statistical significance. The control group-maintained baseline ALT activity levels, while CCl_4 treatment resulted in significantly elevated ALT activity compared to controls (p = 0.0001). ZnO-NP co-treatment demonstrated ALT levels that were significantly elevated compared to controls (p = 0.0002) but significantly lower than the CCl_4 group (p = 0.0006), indicating partial protection. ZnO-NP post-treatment achieved ALT levels that were statistically comparable to the CCl4 group, showing significant differences from baseline values (<0.0001).

Table 3: Effects of ZnO-NP treatment on liver function parameters in the CCl_4-induced hepatotoxicity models.

Parameters	Experimental Groups (Means ± SD)			
	CONTROL	CCl4	ZnO-NP CO.	ZnO-NP POST
ALT(U/L)	31 ± 7.6^{c}	79.5 ± 7.1^{a}	56.4 ± 8.1^{b}	37.7 ± 4^{c}
AST(U/L)	60.2 ± 10.3^{b}	126.5 ± 19.8^{a}	100.7 ± 17^{a}	66.2 ± 10^{b}
ALP(U/L)	89.4 ± 21.6^{b}	221.8 ± 53.1^{a}	122.1 ± 21.4^{b}	80.1 ± 10.6^{b}
Bilirubin (mg/dl)	0.120 ± 0.020^{a}	0.220 ± 0.037^{a}	0.120 ± 0.020^{a}	0.140 ± 0.024^{a}

Values are expressed as means ± standard deviation (n = 5 animals per group). The same letter in the rows denotes no significant differences among parameters at P<0.05, a combination of letters (e.g., ab) indicates no significant differences from groups labeled either a or b, CCl4: carbon tetrachloride group; ZnO-NP CO.: zinc oxide co-treatment group; ZnO-NP POST: zinc oxide post-treatment group. ALT: alanine aminotransferase; AST: aspartate aminotransferase; ALP: alkaline phosphatase.

Control animals exhibited normal AST levels, whereas CCl_4 administration produced significantly elevated AST activity compared to controls (p = 0.0001). ZnO-NP co-treatment resulted in AST levels that were significantly higher than those of controls but showed no statistically significant difference from the CCl4-treated group (p = 0.07). ZnO-NP post-treatment demonstrated AST activity that was statistically comparable to the CCl4 group (p = 0.0001), indicating successful hepatoprotection.

The control group maintained physiological ALP levels, while CCl_4 treatment induced significantly elevated ALP activity compared to controls (p = 0.0001). ZnO-NP co-treatment showed ALP levels that were significantly different from controls but statistically comparable to the CCl_4 group (p = 0.0009). ZnO-NP post-treatment achieved complete restoration of ALP activity to levels statistically similar to the control group (p = 0.97) and significantly differ from CCl4 group (p <0.0001)

CCl_4 administration resulted in a nonsignificant elevation in serum bilirubin concentrations compared to control animals (p = 0.18). ZnO-NP co-treatment-maintained bilirubin levels that were statistically comparable to the control group (p = 0.99), demonstrating effective prevention of hyperbilirubinemia. ZnO-NP post-treatment also preserved bilirubin concentrations that were statistically similar to controls (p = 0.99), indicating successful hepatic function preservation.

The statistical analysis revealed that ZnO-NP post-treatment consistently restored all liver function parameters to levels statistically comparable to controls, while co-treatment provided variable protection depending on the specific biomarker evaluated.

Histopathological Examination of Hepatic Tissue:

Microscopic examination of hepatic tissue sections revealed distinct morphological changes across experimental groups (Figure 6). Control group specimens demonstrated normal hepatic architecture, with intact hepatocytes arranged in characteristic radial cords around central veins, well-defined cellular boundaries, and patent sinusoidal spaces without inflammatory infiltration or pathological alterations.

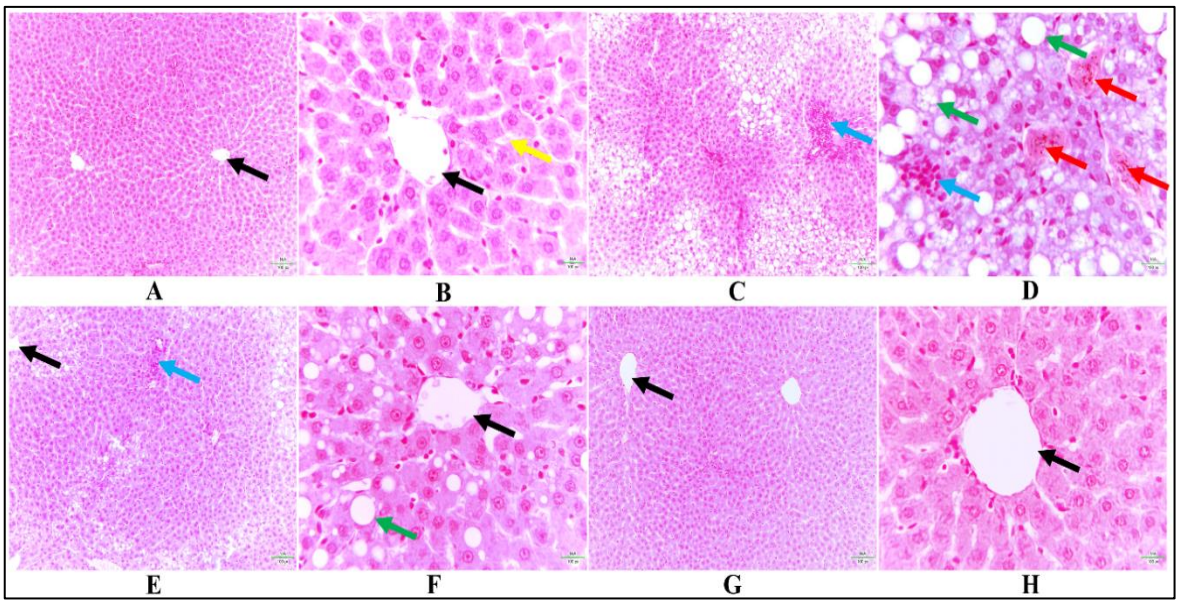

Figure. 6: Histological sections of liver tissue stained with H&E showing the effects of CCl_4 and ZnO-NP treatments. (A, B) Control group: normal hepatic architecture with normal sinusoids (yellow arrow) and central vein (black arrows). (C, D) CCl_4 group: severe hepatocellular degeneration and steatosis with lipid droplets (green arrows), dilated sinusoids (red arrows), and inflammatory cell infiltration (blue arrows). (E, F) ZnO-NP co-treatment: partial liver protection with mild inflammation (blue arrows) and lipid accumulation (green arrow). (G, H) ZnO-NP post-treatment: near-normal architecture indicating regeneration with restored sinusoidal structure. Magnifications: A, C, E, G (×100); B, D, F, H (×400)

CCl_4 treatment induced severe hepatotoxicity characterized by extensive hepatocellular ballooning degeneration and massive macrovesicular steatosis with lipid droplets. Significant inflammatory cell infiltration consisting of neutrophils and lymphocytes was observed around necrotic areas and portal regions, accompanied by sinusoidal congestion and complete disruption of normal hepatic cord architecture.

ZnO-NP co-treatment provided substantial hepatoprotection with markedly reduced tissue damage compared to the CCl_4-alone group. Ballooning degeneration was mild to moderate and confined to scattered hepatocytes, while steatotic changes were predominantly microvesicular lipid droplets. The inflammatory response was considerably attenuated with only focal collections around portal areas, and necrotic areas were rare and small. Hepatic lobular architecture showed good preservation with recognizable hepatic cords.

ZnO-NP post-treatment exhibited exceptional hepatic regeneration virtually indistinguishable from controls. Complete restoration of normal hepatocyte morphology with abundant eosinophilic cytoplasm, perfect hepatic lobular architecture, and complete resolution of steatosis was achieved. Inflammatory response was minimal, comparable to control levels, with no histological evidence of necrosis or ballooning degeneration, indicating complete tissue recovery and well-organized hepatic regeneration.

4. DISCUSSION

The present investigation demonstrates the exceptional hepatoprotective efficacy of verjuice (Unripe Grape juice, *Vitis vinefera* L.) -synthesized ZnO-NPs against CCl_4-induced liver toxicity, with post-treatment protocols showing superior therapeutic outcomes compared to concurrent treatment approaches. The dose of 50 mg/kg ZnO-NP was selected based on prior rodent studies showing both biological efficacy and tolerable safety. For instance, immunotoxicology and hepatic–renal toxicity assessments in Wistar rats and BALB/c mice revealed that 50 mg/kg ZnO-NP elicited measurable oxidative and inflammatory responses without severe organ damage when compared to higher doses (e.g., 100–200 mg/kg) (Abbasalipourkabir *et, al.*, 2015).

UV-visible spectroscopy revealed characteristic absorption at 372 nm, with an optical band gap of 3.32 eV, confirming ZnO-NP formation and semiconductor properties essential for biological activity (Gulab *et, al.*, 2024). These findings align with research demonstrating that green-synthesized ZnO-NPs exhibit superior biocompatibility and enhanced therapeutic properties compared to chemically synthesized counterparts (Ashraf *et, al.*, 2023). The XRD characterization confirms the successful synthesis of pure wurtzite ZnO-NPs, as evidenced by the characteristic diffraction peaks corresponding to the hexagonal crystal structure. The crystallite size analysis, derived from line broadening of the most intense peak, yielded an average value of 53.1 nm, indicating the formation of well-defined nanocrystalline particles. This crystalline purity and absence of secondary phases suggest that the green synthesis approach effectively maintains structural integrity while providing an environmentally sustainable synthetic route. These findings are consistent with recent comprehensive reviews demonstrating that green synthesis methodologies produce ZnO-NPs with superior properties compared to conventional chemical synthesis approaches (Naser *et, al.*, 2023; El-Saadony *et, al.*, 2024; Sameri *et, al.*, 2024).

The distinctive flower-like morphology observed in SEM analysis represents a unique structural configuration that enhances surface area and cellular interaction, as supported by recent studies showing morphology-dependent therapeutic

efficacy (Udayagiri *et al.*, 2024). The discrepancy between XRD crystallite size (53.1 nm) and SEM particle size (~85 nm) likely reflects nanoparticle agglomeration or multi-crystallite structures, which are common in green-synthesized materials. FTIR analysis confirmed the presence of organic capping agents from verjuice extract, indicating successful bio-functionalization. This aligns with research demonstrating that plant-derived stabilizing agents enhance nanoparticle stability and bioactivity (Fiedot-Toboła *et al.*, 2021). The green synthesis approach incorporating polyphenolic compounds provides synergistic therapeutic effects beyond the nanoparticle core activity, as seen in studies investigating grape pomace-mediated nanoparticle synthesis (Saratale *et al.*, 2020). EDX analysis confirmed elemental composition with characteristic peaks for zinc and oxygen, indicating high purity (9). This green synthesis approach offers enhanced biocompatibility by incorporating polyphenolic compounds that provide synergistic therapeutic effects beyond the nanoparticle core activity (Angle, 2024; Verma *et al.*, 2021).

The antioxidant enzyme activities analysis revealed ZnO-NPs' primary hepatoprotective mechanism through sophisticated preservation of cellular antioxidant systems. SOD activity showed complete restoration in the post-treatment group (functional recovery), while MDA levels were effectively normalized, demonstrating prevention of lipid peroxidation. These findings strongly support recent studies demonstrating similar hepatoprotective effects of green-synthesized ZnO-NPs from Moringa oleifera leaves in CCl_4-treated rats, showing significant preservation of antioxidant enzyme activities (El-Beltagi *et al.*, 2024).

Recent research has provided comprehensive evidence supporting ZnO-NP's antioxidant capabilities through zinc's role as an essential cofactor for Cu/Zn-SOD function. The selective preservation of enzymatic antioxidant pathways observed in our study aligns with previous findings demonstrating ZnO-NPs ability to ameliorate oxidative stress through apoptotic gene regulation in liver ischemia-reperfusion injury models (Sameri *et al.*, 2024).

The maintained GSH levels across all treatment groups suggest that ZnO-NPs operate through selective enzymatic rather than non-enzymatic antioxidant pathways, supporting the mechanism proposed regarding the targeted antioxidant effects of green-synthesized ZnO-NPs (Verma *et al.*, 2021). The absence of significant changes in GSH may also reflect early compensatory mechanisms or methodological limitations in detecting subtle shifts in non-enzymatic antioxidant capacity. Substantial contradictory literature demonstrates ZnO-NP-induced oxidative stress and hepatotoxicity, presenting a significant challenge to our findings. Multiple studies report dose-dependent decreases in SOD, CAT, and GPx activities alongside increased MDA levels, directly opposing our results (Ansar *et al.*, 2018; Bayat *et al.*, 2023; Khorsandi *et al.*, 2016; Kausar *et al.*, 2023).

Weight gain analysis revealed severe hepatotoxicity-induced growth retardation in the CCl_4 group (57.2% reduction), while ZnO-NP post-treatment achieved remarkable recovery equivalent to 103.7% of control levels. This finding is supported by recent studies demonstrating successful weight recovery following nanoparticle interventions (Kazmi *et al.*, 2021; Mostafa-Hedeab *et al.*, 2023), though other investigations reported persistent weight deficits, suggesting that complete recovery may not always be achievable (Mosquera-Murillo *et, al.*, 2023).

These biochemical findings highlight distinct patterns of hepatic injury and protection. The marked elevation of ALT activity following CCl_4 administration confirms severe hepatocellular damage, consistent with its well-known hepatotoxic mechanism. The partial reduction of ALT levels with ZnO-NP co-treatment suggests that simultaneous administration offers some degree of protection, though not complete recovery. Notably, the complete normalization of ALT activity observed with ZnO-NP post-treatment indicates that green-synthesized nanoparticles can effectively promote hepatic regeneration and restore liver enzyme balance when administered after injury.

Similar patterns were observed for AST activity, where CCl_4 administration produced marked elevations indicative of hepatocellular injury. ZnO-NP co-treatment provided limited protection for AST levels, while ZnO-NP post-treatment demonstrated complete restoration of AST activity to normal physiological ranges, indicating successful prevention of hepatocellular damage.

Alkaline phosphatase activity followed comparable trends, with CCl_4 treatment inducing significant elevations reflecting hepatobiliary dysfunction. ZnO-NP co-treatment showed modest protective effects, while ZnO-NP post-treatment achieved complete restoration of ALP activity to baseline levels, suggesting full recovery of hepatobiliary function. These findings are supported by recent studies demonstrating ZnO-NPs' ability to improve liver function in ischemia-reperfusion injury models, with significant reductions in liver enzyme elevations (Awadalla *et al.*, 2021; Sameri *et al.*, 2024).

However, substantial contradictory evidence challenges the conventional safety of ZnO-NPs. Recent studies demonstrate that chemically synthesized ZnO-NPs induce hepatotoxicity with elevated liver enzymes, inflammatory responses, and oxidative stress at doses comparable to our therapeutic range (Herrera-Rodríguez *et al.*, 2023; Kausar *et al.*, 2023; Pei *et al.*, 2023). These findings contradict our observations of hepatoprotection and enzyme normalization, suggesting that green synthesis methodology fundamentally alters nanoparticle biocompatibility. The superior therapeutic efficacy of our verjuice-synthesized ZnO-NPs may result from unique phytochemical surface modifications that distinguish it from conventionally prepared particles, highlighting green synthesis as a critical factor in developing safe nanotherapeutics.

Histopathological examination revealed distinct morphological changes across experimental groups. Control specimens demonstrated normal hepatic architecture with intact hepatocytes arranged in characteristic radial cords. CCl_4 treatment induced severe hepatotoxicity characterized by extensive hepatocellular ballooning degeneration, massive macrovesicular steatosis, and widespread coagulative necrosis. ZnO-NP post-treatment exhibited exceptional hepatic regeneration virtually indistinguishable from controls, with complete restoration of normal hepatocyte morphology and complete resolution of steatosis. Recent studies supporting our findings include investigations showing ZnO-NPs' role in liver regenerative therapy and tissue restoration (Al Sulivany *et al.,* 2024*;* Gupta *et al.,* 2023; Park *et al.,* 2025; Sameri *et al.*, 2024). A limitation of this study is the small sample size (n = 5 per group), which may reduce the statistical power and limit the generalizability of the findings. Another limitation of this study

is the use of a single ZnO-NP dose without a dose–response assessment, which precludes the determination of the minimum effective or toxic dose and the precise therapeutic window. Although our results show liver recovery, we did not assess potential off-target toxicity in other organs. Further studies should include renal and hematological parameters to ensure systemic safety of green-synthesized ZnO-NPs.

CONCLUSION

This study establishes verjuice-synthesized ZnO-NPs as highly effective hepatoprotective agents against CCl_4-induced toxicity. Post-treatment protocols achieved complete antioxidant enzyme restoration, comprehensive liver enzyme normalization, and full morphometric recovery. The green synthesis approach provides environmental sustainability while enhancing therapeutic efficacy through bioactive phytochemical coating. These findings warrant clinical investigation for drug-induced liver injury, though contradictory toxicity evidence necessitates extensive safety studies before clinical translation. This research represents a significant advancement in nanomedicine-based therapeutic strategies, demonstrating remarkable hepatic regeneration even after established toxic.

Acknowledgement:

The authors express their sincere gratitude to Dr. Safin H. Hussein for his valuable guidance, constructive feedback, and continuous support throughout this research.

Ethical Statement:

The animal experimentation protocol was conducted in strict accordance with international guidelines for animal welfare and was approved by the Ethics Committee of Salahaddin University College of Education (Approval Code: SU2025AREC/17).

Author Contributions:

P. A. conducted the experimental work, data collection, and analysis, and wrote the manuscript as part of her master's degree research. T. I., designed the study methodology, conceptualized the work, and provided supervision and editorial review. Both P. A. and T. I. approved the final manuscript and agree to be accountable for all aspects of the work.

REFERENCES

Abbasalipourkabir, R., Moradi, H., Zarei, S., Asadi, S., Salehzadeh, A., Ghafourikhosroshahi, A., Ziamajidi, N. (2015). Toxicity of zinc oxide nanoparticles on adult male Wistar rats. *Food and chemical toxicology, 84*, 154-160: https://doi.org/10.1016/j.fct.2015.08.019.

Adeyemi, J. O., Oriola, A. O., Onwudiwe, D. C., & Oyedeji, A. O. (2022). Plant extracts mediated metal-based nanoparticles: synthesis and biological applications. *Biomolecules, 12*(5), 627: http://doi.org/10.3390/biom12050627.

Al-Sulivany, B., Ahmed, D., Naif, R., Saleem, P., & Omer, E. (2024). Phytochemical Profile of Eruca sativa and Its Therapeutic Potential in Disease Prevention and Treatment. *Global Academic Journal of Agriculture and Biosciences, 6*(3), 57-64: http://doi.org/10.36348/gajab.2024.v06i03.002

Al Sulivany, B. S., Abdulla, I. T., Mohammed, C. M., Shaheen, M. S., Hassan, M. M., & Salih, S. J. (2024). Spirulina (*arthrospora platensis*) in the diet reduces sodium arsenates' impacts on kidney enzyme activities, histopathology, and arsenic accumulation in rats models. *Egyptian Academic Journal of Biological Sciences, D. Histology & Histochemistry, 16*(1), 1-10: https://doi.org/10.21608/eajbsd.2024.333813.

Alipour, M., Davoudi, P., & Davoudi, Z. (2012). Effects of unripe grape juice (verjuice) on plasma lipid profile, blood pressure, malondialdehyde and total antioxidant capacity in normal, hyperlipidemic and hyperlipidemic with hypertensive human volunteers. *Journal of Medicinal Plants Research, 6*(45), 5677-5683: http://doi.org/10.5897/JMPR11.1146.

Angle, A. S. (2024). Green Synthesis Methods for Metallic Zinc Oxide Nanoparticles. *Synthesizing and Characterizing Plant-Mediated Biocompatible Metal Nanoparticles*, 63:

Ansar, S., Abudawood, M., Alaraj, A. S., & Hamed, S. S. (2018). Hesperidin alleviates zinc oxide nanoparticle induced hepatotoxicity and oxidative stress. *BMC Pharmacology and Toxicology, 19*, 1–6: http://DOI.org/10.1186/s40360-018-0256-8.

Ashraf, H., Meer, B., Iqbal, J., Ali, J. S., Andleeb, A., Butt, H. Drouet, S. (2023). Comparative evaluation of chemically and green synthesized zinc oxide nanoparticles: their in vitro antioxidant, antimicrobial, cytotoxic and anticancer potential towards HepG2 cell line. *Journal of Nanostructure in Chemistry, 13*(2), 243-261: http://doi.org/10.1007/s40097-021-00460-3.

Awadalla, A., Hussein, A. M., Yousra, M., Barakat, N., Hamam, E. T., El-Sherbiny, M., Shokeir, A. A. (2021). Effect of zinc oxide nanoparticles and ferulic acid on renal ischemia/reperfusion injury: possible underlying mechanisms. *Biomedicine & Pharmacotherapy, 140*, 111686: https://doi.org/10.1016/j.biopha.2021.111686.

Bayat, M., Daei, S., Ziamajidi, N., Abbasalipourkabir, R., & Nourian, A. (2023). The protective effects of vitamins A, C, and E on zinc oxide nanoparticles (ZnO NPs)-induced liver oxidative stress in male Wistar rats. *Drug Chem Toxicol, 46*(2), 209-218: https://doi.org/10.1080/01480545.2021.2016809.

Bayram, Y., & Elgin Karabacak, C. (2022). Characterization of unripe grapes (*Vitis vinifera L.*) and its use to obtain antioxidant phenolic compounds by green extraction. *Frontiers in Sustainable Food Systems, 6*, 909894: https://doi.org/10.3389/fsufs.2022.909894.

Conde de la Rosa, L., Goicoechea, L., Torres, S., Garcia-Ruiz, C., & Fernandez-Checa, J. C. (2022). Role of oxidative stress in liver disorders. *Livers, 2*(4), 283-314: https://doi.org/10.3390/livers2040023.

Datta, S., Aggarwal, D., Sehrawat, N., Yadav, M., Sharma, V., Sharma, A., Kumar, V. (2023). Hepatoprotective effects of natural drugs: Current trends, scope, relevance and future perspectives. *Phytomedicine, 121*, 155100: https://doi.org/10.1016/j.phymed.2023.155100.

Dhalaria, R., Verma, R., Kumar, D., Puri, S., Tapwal, A., Kumar, V., Kuca, K. (2020). Bioactive compounds of edible fruits with their anti-aging properties: A comprehensive review to prolong human life. *Antioxidants, 9*(11), 1123: https://doi.org/10.3390/antiox9111123.

Dohadwala, M. M., & Vita, J. A. (2009). Grapes and cardiovascular disease. *The Journal of nutrition, 139*(9), 1788S-1793S: https://doi.org/10.3945/jn.109.107474.

El-Beltagi, H. S., Rageb, M., El-Saber, M. M., El-Masry, R. A., Ramadan, K. M., Kandeel, M.,Osman, A. (2024). Green synthesis, characterization, and hepatoprotective effect of zinc oxide nanoparticles from Moringa oleifera leaves in CCl4-treated albino rats. *Heliyon, 10*(9): https://doi.org/10.1016/j.heliyon.2024.e30627.

El-Saadony, M. T., Fang, G., Yan, S., Alkafaas, S. S., El Nasharty, M. A., Khedr, S. A., Elkafas, S. S. (2024). Green Synthesis of Zinc Oxide Nanoparticles: Preparation, Characterization, and Biomedical Applications-A Review. *International Journal of Nanomedicine*, 12889-12937: https://doi.org/10.2147/IJN.S487188.

Fazal, R. M., Kaynat, F., Rizwan, P., Al Sulivany, B., & Owais, M. (2024). Harnessing isosaponarin: A multifaceted bioactive and therapeutic potential compound from nature. *Biological and Biomedical Journal*: http://doi.org/10.21608/bbj.2024.331198.1047

Fiedot-Toboła, M., Dmochowska, A., Potaniec, B., Czajkowska, J., Jędrzejewski, R., Wilk-Kozubek, M., Cybińska, J. (2021). Gallic acid based black tea extract as a stabilizing agent in ZnO particles green synthesis. *Nanomaterials, 11*(7), 1816: https://doi.org/10.3390/nano11071816.

Gong, Z., Yan, S., Zhang, P., Huang, Y., & Wang, L. (2008). Effects of S-adenosylmethionine on liver methionine metabolism and steatosis with ethanol-induced liver injury in rats. *Hepatol Int, 2*(3), 346-352: http://doi.org/10.1007/s12072-008-9082-1.

Gulab, H., Fatima, N., Tariq, U., Gohar, O., Irshad, M., Khan, M. Z., Jan, A. K. (2024). Advancements in zinc oxide nanomaterials: synthesis, properties, and diverse applications. *Nano-Structures & Nano-Objects, 39*, 101271: https://doi.org/10.1016/j.nanoso.2024.101271.

Gupta, J., Hassan, P., & Barick, K. (2023). Multifunctional ZnO nanostructures: a next generation nanomedicine for cancer therapy, targeted drug delivery, bioimaging, and tissue regeneration. *Nanotechnology, 34*(28), 282003: http://DOI.org/10.1088/1361-6528/accc35.

Gupta, N., Gupta, D., & Sharma, P. (2017). Condition factor and organosomatic indices of parasitized Rattus rattus as indicators of host health. *Journal of parasitic diseases, 41*(1), 21-28: https://doi.org/10.1007/s12639-015-0744-3.

Hashim, M., Anjum, S., Mujahid, H., Alotaibi, K. S., Albattal, S. B., Ghamry, H. I., & Soliman, M. M. (2025). Thymoquinone loaded zinc oxide Nanoformulations synthesis, characterization and evaluation of their efficacy against carbon tetrachloride induced Hepatorenal toxicity in rats. *Toxicology Research, 14*(2), tfaf037: https://doi.org/10.1093/toxres/tfaf037.

Herrera-Rodríguez, M. A., del Pilar Ramos-Godinez, M., Cano-Martínez, A., Segura, F. C., Ruiz-Ramírez, A., Pavón, N., Delgado-Buenrostro, N. L. (2023). Food-grade titanium dioxide and zinc oxide nanoparticles induce toxicity and cardiac damage after oral exposure in rats. *Particle and Fibre Toxicology, 20*(1), 43: https://doi.org/10.1186/s12989.

Kausar, S., Jabeen, F., Latif, M. A., & Asad, M. (2023). Characterization, dose dependent assessment of hepatorenal oxidative stress, hematological parameters and histopathological divulging of the hepatic damages induced by Zinc oxide nanoparticles (ZnO-NPs) in adult male Sprague Dawley rats. *Saudi Journal of Biological Sciences, 30*(9), 103745: https://doi.org/10.1016/j.sjbs.2023.103745.

Kazmi, I., Al-Abbasi, F. A., Afzal, M., Altayb, H. N., Nadeem, M. S., & Gupta, G. (2021). Formulation and evaluation of kaempferol loaded nanoparticles against experimentally induced hepatocellular carcinoma: in vitro and in vivo studies. *Pharmaceutics, 13*(12), 2086: https://doi.org/10.3390/pharmaceutics13122086.

Khorsandi, L., Mansouri, E., Orazizadeh, M., & Jozi, Z. (2016). Curcumin Attenuates Hepatotoxicity Induced by Zinc Oxide Nanoparticles in Rats. *Balkan Med J, 33*(3), 252-257: http://doi.org/10.5152/balkanmedj.2016.150017.

Kirubakaran, D., Wahid, J. B. A., Karmegam, N., Jeevika, R., Sellapillai, L., Rajkumar, M., & SenthilKumar, K. (2025). A comprehensive review on the green synthesis of nanoparticles: advancements in biomedical and environmental applications. *Biomedical Materials & Devices*, 1-26: https://doi.org/10.1007/s44174-025-00295-4.

Marrocco, I., Altieri, F., & Peluso, I. (2017). Measurement and clinical significance of biomarkers of oxidative stress in humans. *Oxidative medicine and cellular longevity, 2017*(1), 6501046: https://doi.org/10.1155/2017/6501046

Mohajan, H. K. (2025). A Study on Functions of Liver to Sustain a Healthy Liver. *Innovation in Science and Technology, 4*(1), 77-87: http://doi.org/10.56397/IST.2025.01.08.

MohamedAmin, P. J. (2024). Formaldehyde vapor-induced chronic tracheitis in relation to the expression of S-100 proteins. *Zanco Journal of Medical Sciences (Zanco J Med Sci), 28*(1), 61-72: https://doi.org/10.15218/zjms.2024.007.

Mohi-Ud-Din, R., Mir, R. H., Sawhney, G., Dar, M. A., & Bhat, Z. A. (2019). Possible pathways of hepatotoxicity caused by chemical agents. *Current drug metabolism, 20*(11), 867-879: https://doi.org/10.2174/1389200220666191105121653.

Mosquera-Murillo, K., Castañeda-Manquillo, A., Ángel-Camilo, K., Arciniegas-Grijalba, P., de Valdenebro, M. R., Mosquera-Sanchez, L., . . . Rodriguez-Paez, J. (2023). Evaluation of the toxicity of ZnO nanoparticles obtained by a chemical route on the nasal respiratory epithelium of the biomodel Mus musculus. *Journal of Nanoparticle Research, 25*(12), 258: https://doi.org/10.1007/s11051-023-05902-3.

Mostafa-Hedeab, G., Behairy, A., Abd-Elhakim, Y. M., Mohamed, A. A.-R., Noreldin, A. E., Dahran, N., Eskandrani, A. A. (2023). Green synthesized zinc oxide nanoparticles using moringa olifera ethanolic extract lessens acrylamide-induced testicular damage, apoptosis, and steroidogenesis-related gene dysregulation in adult rats. *Antioxidants, 12*(2), 361: https://doi.org/10.3390/antiox12020361.

Naser, S. S., Ghosh, B., Simnani, F. Z., Singh, D., Choudhury, A., Nandi, A., Suar, M. (2023). Emerging trends in the application of green synthesized biocompatible ZnO nanoparticles for translational paradigm in cancer

therapy. *Journal of Nanotheranostics, 4*(3), 248-279: https://doi.org/10.3390/jnt4030012.

Nematbakhsh, M., Zolfaghari, B., Eshraghi, F., Safari, T., Pezeshki, Z., & Sorooshzadeh, S. M.-A. (2013). The effects of unripe grape extract on systemic blood pressure, nitric oxide production, and response to angiotensin II administration. *Pharmacognosy research, 5*(2), 60: https://doi.org/10.4103/0974-8490.110511.

Park, N., Kim, K. S., Lee, S., Choi, J. H., & Na, K. (2025). Enhanced stem cell-mediated therapeutic immune modulation with zinc oxide nanoparticles in liver regenerative therapy. *Biomaterials, 320*, 123232: https://doi.org/10.1016/j.biomaterials.2025.123232.

Pei, X., Tang, S., Jiang, H., Zhang, W., Xu, G., Zuo, Z., Li, C. (2023). Paeoniflorin recued hepatotoxicity under zinc oxide nanoparticles exposure via regulation on gut-liver axis and reversal of pyroptosis. *Science of the Total Environment, 904*, 166885: https://doi.org/10.1016/j.scitotenv.2023.166885.

Salah Eddine, N., Tlais, S., Alkhatib, A., & Hamdan, R. (2020). Effect of four grape varieties on the physicochemical and sensory properties of unripe grape verjuice. *International Journal of Food Science, 2020*(1), 6457982: https://doi.org/10.1155/2020/6457982.

Sameri, M. J., Savari, F., Mard, S. A., Rezaie, A., & Kalantar, M. (2024). Zinc Oxide Nanoparticles Ameliorate Histological Alterations Through Apoptotic Gene Regulation in Rat Model of Liver Ischemia-Reperfusion Injury. *Reports of biochemistry & molecular biology, 12*(4), 619: https://doi.org/10.61186/rbmb.12.4.619.

Saratale, G. D., Saratale, R. G., Kim, D.-S., Kim, D.-Y., & Shin, H.-S. (2020). Exploiting fruit waste grape pomace for silver nanoparticles synthesis, assessing their antioxidant, antidiabetic potential and antibacterial activity against human pathogens: a novel approach. *Nanomaterials, 10*(8), 1457: https://doi.org/10.3390/nano10081457.

Szymonik-Lesiuk, S., Czechowska, G., Stryjecka-Zimmer, M., Słomka, M., MĄldro, A., Celiński, K., & Wielosz, M. (2003). Catalase, superoxide dismutase, and glutathione peroxidase activities in various rat tissues after carbon tetrachloride intoxication. *Journal of hepato-biliary-pancreatic surgery, 10*, 309-315: https://doi.org/10.1007/s00534-002-0824-5.

Udayagiri, H., Sana, S. S., Dogiparthi, L. K., Vadde, R., Varma, R. S., Koduru, J. R., Kim, S.-C. (2024). Phytochemical fabrication of ZnO nanoparticles and their antibacterial and anti-biofilm activity. *Scientific Reports, 14*(1), 19714: https://doi.org/s41598-024-69044-9.

Verma, R., Pathak, S., Srivastava, A. K., Prawer, S., & Tomljenovic-Hanic, S. (2021). ZnO nanomaterials: Green synthesis, toxicity evaluation and new insights in biomedical applications. *Journal of Alloys and Compounds, 876*, 160175: https://doi.org/10.1016/j.jallcom.2021.160175.

Wazir, H., Abid, M., Essani, B., Saeed, H., Khan, M. A., Nasrullah, F., Muzammil, M. A. (2023). Diagnosis and treatment of liver disease: current trends and future directions. *Cureus, 15*(12): http://doi.org/10.7759/cureus.49920.

Weber, L. W., Boll, M., & Stampfl, A. (2003). Hepatotoxicity and mechanism of action of haloalkanes: carbon tetrachloride as a toxicological model. *Critical reviews in toxicology, 33*(2), 105-136: https://doi.org/10.1080/713611034.

Zhao, D., Simon, J. E., & Wu, Q. (2020). A critical review on grape polyphenols for neuroprotection: Strategies to enhance bioefficacy. *Critical Reviews in Food Science and Nutrition, 60*(4), 597-625: https://doi.org/10.1080/10408398.2018.1546668.

Zhou, D.-D., Li, J., Xiong, R.-G., Saimaiti, A., Huang, S.-Y., Wu, S.-X., Gan, R.-Y. (2022). Bioactive compounds, health benefits and food applications of grape. *Foods, 11*(18), 2755: https://doi.org/10.3390/foods11182755.